

respirators and fermenters, respectively. Assuming a yield of 32 mol of ATP per mole of glucose, the ATP production of respiration is given by $J_1^{ATP}(S) = 32J_2^R(S)$. In fermentation the remainder of the resource uptake, $J_2^F(S) - J_2^R(S)$, is fermented with a yield of 2 ATP. Thus, the total ATP production of a fermenter is given by $J_2^{ATP}(S) = 32J_2^R(S) + 2[J_2^F(S) - J_2^R(S)]$. For computer simulations, the model (Eq. 2) was transformed into the corresponding difference equations [W. H. Press, S. A. Teukolsky, W. T. Vetterling, B. P. Flannery, *Numerical Recipes* (Cambridge Univ. Press, Cambridge, ed. 2, 1992)]. All simulations were performed on a 100×100 grid (except for the 200×200 grid in Fig. 1B) with a grid unit length of 1 and a time step of 0.001. In all simulations we chose $c = 1$, $d = 10$, and $D^S = 1$. An amount of resource, R , was added to a site stochastically with a probability of 0.0005 per time step. N_i was rounded up or down probabilistically (with p and $p - 1$, respectively, where p is the fractional part of N_i) to

reflect discrete cell numbers. All simulations were started with fermenting cells only. Between time steps 50,000 and 100,000, respiring cells were added with probability 10^{-5} per site and time step. The population size shown in Fig. 1C was averaged over time steps 200,000 to 250,000.

28. P. J. Rogers, G. D. Clark-Walker, P. R. Stewart, *J. Bacteriol.* **119**, 282 (1974).
29. B. E. Schulz, G. Kraepelin, W. Hinkelmann, *J. Gen. Microbiol.* **82**, 1 (1974).
30. L. Margulis, *Symbiosis in Cell Evolution* (Freeman, San Francisco, 1981).
31. R. E. Dickerson, *Sci. Am.* **242**, 137 (March 1980).
32. J. T. Bonner, *Integrat. Biol.* **1**, 27 (1998).
33. J. Maynard Smith, E. Szathmáry, *The Major Transitions in Evolution* (Freeman, Oxford, 1995).
34. We argue that aggregation of cells and the formation of multicellular organisms allowed cells to benefit from the high ATP yield resulting from the exclusive use of respiration. This is in contrast to the hypoth-

esis that after the evolution of respiration, the high ATP yield of respiration gave cells an "energetic luxury" that subsequently allowed them to increase genome size and evolve multicellularity [T. Vellai, K. Takács, G. Vida, *J. Mol. Evol.* **46**, 499 (1998)].

35. Our line of reasoning only applies to heterotrophic organisms, because it is based on competition for an exhaustible resource and a trade-off between rate and yield of ATP production. In phototrophic organisms there is no evolutionary dilemma, because light is an inexhaustible resource. As a consequence, phototrophic organisms need not overcome this evolutionary dilemma for the evolution of multicellularity.
36. We thank M. Ackermann, M. Brown, M. Flor, T. Killingback, D. Krakauer, and P. Schmid-Hempel for helpful discussions and critical review of the manuscript. Support from the Novartis Research Foundation (T.P. and S.B.) and the Deutsche Forschungsgemeinschaft (S.S.) is gratefully acknowledged.

7 December 2000; accepted 2 March 2001

astray, a Zebrafish roundabout Homolog Required for Retinal Axon Guidance

Cornelia Fricke,¹ Jeong-Soo Lee,¹ Silke Geiger-Rudolph,² Friedrich Bonhoeffer,³ Chi-Bin Chien^{1*}

As growing retinotectal axons navigate from the eye to the tectum, they sense guidance molecules distributed along the optic pathway. Mutations in the zebrafish *astray* gene severely disrupt retinal axon guidance, causing anterior-posterior pathfinding defects, excessive midline crossing, and defasciculation of the retinal projection. Eye transplantation experiments show that *astray* function is required in the eye. We identify *astray* as zebrafish *robo2*, a member of the Roundabout family of axon guidance receptors. Retinal ganglion cells express *robo2* as they extend axons. Thus, *robo2* is required for multiple axon guidance decisions during establishment of the vertebrate visual projection.

During development of the retinotectal projection, retinal ganglion cell (RGC) axons navigate through a series of environments. They first grow toward the optic disc, exit the eye at the ventral fissure, and grow along the base of the ventral diencephalon, where they meet the contralateral retinal axons, forming the optic chiasm. They then progress into the optic tract and project topographically to their central targets, primarily the optic tectum in nonmammalian vertebrates. There is a growing understanding of the molecular mechanisms that specify retinotectal topography (1–3) and that guide retinal axons within the eye (4, 5), but to date few axon guidance molecules have been shown in vivo to function

between eye and tectum (6, 7).

We have used the zebrafish to identify such guidance molecules and study their functions in vivo. The transparency of the larvae in combination with the amenability of this model organism to genetics has made it possible to directly visualize the retinal projection and isolate genes required for RGC axon guidance (8). *astray* (*ast*) (9) is one of the key genes isolated in this large-scale screen. Four alleles (*ti272z*, *te378*, *tl231*, and *te284*) have been found, all with similar phenotypes. Compared to wild type (WT), in which the retinotectal projection at 5 days postfertilization (dpf) is exclusively contralateral, RGC axons in *ast/ast* embryos exhibited misprojections to ipsilateral tectum and several extraretinal targets (9) (Fig. 1).

Confocal analysis after lipophilic dye labeling at 5 dpf (10) showed that after *ast* RGC axons exited the eye, they made a wide variety of pathfinding errors at multiple locations (Fig. 1), predominantly at or after the midline. Anterior-posterior guidance defects were common, including anterior projections into diencephalon and telencephalon, and posterior projections to both ipsilateral and

contralateral ventral hindbrain (VHB) (Fig. 1, C to F). Anteriorly projecting axons often reached as far as presumptive olfactory bulb; they also often recrossed the midline, then continued anteriorly or turned posteriorly (Fig. 1E). Axons recrossed the midline in at least three distinct locations: VHB, ventral telencephalon near the anterior commissure (AC), and dorsally in the posterior commissure (PC); the latter was a common route by which retinal axons reached the ipsilateral tectum (Fig. 1C). In strong phenotypes, the optic tract showed severe defasciculation (Fig. 1, E and F). Occasionally, the optic chiasm formed abnormally: The optic nerve was unusually distant from the contralateral optic nerve, or split into two or more parts at the midline (Fig. 1I). Retinal axons also sometimes projected into the opposite eye. Axons from all four retinal quadrants showed pathfinding errors; however, axons that reached the tectum appeared to project topographically (9, 11). Thus, *ast* function is required for midline crossing as well as several other axon guidance decisions.

All four *ast* alleles are recessive and cause a similar array of phenotypes, suggesting that they are loss-of-function mutations. Phenotypic strength varied widely between embryos, even within clutches, and the two eyes sometimes showed different phenotypes. Even in the embryos with the strongest phenotypes, a subset of axons reached the contralateral tectum. Scoring *ast/+* × *ast/+* incrosses (10) showed three completely penetrant alleles [*ti272z* (24.5% mutant, $n = 335$ embryos), *te378* (25.8%, $n = 159$), and *tl231* (25.3%, $n = 182$)] and one weaker allele [*te284* (18.0%, $n = 133$)]. Supporting the conclusion that *te284* is weaker was the observation that often only a single eye of *te284* homozygotes showed a detectable phenotype, whereas in all *ti272z* homozygotes examined, both eyes showed mutant phenotypes. Projections to VHB (86%) and across the PC (78%) were more common than anterior projections (64%) (*ti272z* homozygotes, $n = 175$ eyes).

¹Department of Neurobiology and Anatomy, University of Utah Medical Center, 50 North Medical Drive, Salt Lake City, UT 84132, USA. Abteilung ²Genetik and ³Physikalische Biologie, Max-Planck Institut für Entwicklungsbiologie, Spemannstrasse 35, D-72076 Tübingen, Germany.

*To whom correspondence should be addressed at Department of Neurobiology and Anatomy, 401 MREB, University of Utah Medical Center, 50 North Medical Drive, Salt Lake City, UT 84132, USA. E-mail: chi-bin.chien@hsc.utah.edu

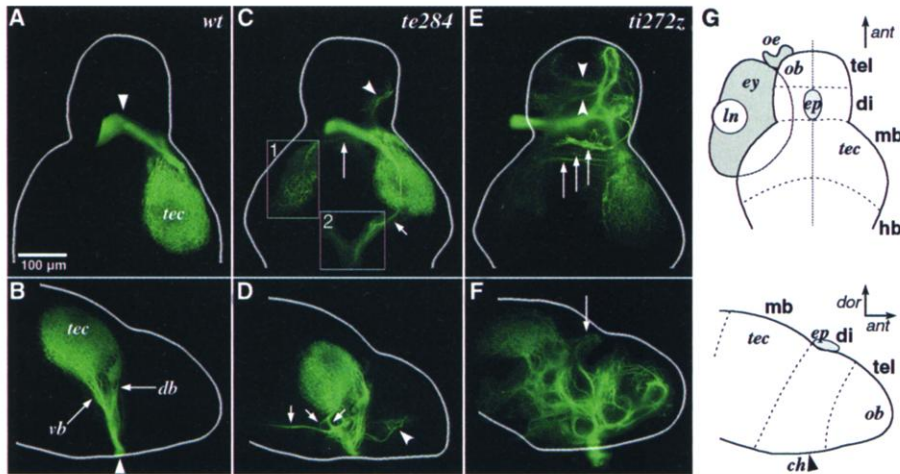


Fig. 1. *ast* mutants show multiple retinal axon guidance defects. (A to F) Three retinal projections are shown in dorsal (A, C, and E) and lateral (B, D, and F) views. Eyes have been removed, and brain outlines are shown in white; boxed insets in (C) are at high gain to reveal faint projections. (G) ant, anterior; dor, dorsal; ch, chiasm; di, diencephalon; ep, epiphysis; ey, eye; hb, hindbrain; ln, lens; mb, midbrain; ob, olfactory bulb; oe, olfactory epithelium; tec, tectum; tel, telencephalon. (A and B) WT axons cross the ventral midline (arrowheads), form the dorsal (db) and ventral (vb) brachia of the optic tract, and arborize in contralateral tectum. (C and D) Weak *ast* phenotype (*te284*). Most axons project normally, but a small fascicle projects anteriorly (arrowheads), and several fibers recross in the PC (long arrow). Of three fascicles that leave the ventral brachium (short arrows), two correct and enter the tectum, whereas the third continues into the VHB. (Inset C1) Fibers recrossing in the PC arborize in the ipsilateral tectum. (Inset C2) Posteriorly projecting fibers recross in the VHB. (E and F) Strong *ast* phenotype (*ti272z*). Few axons reach the contralateral tectum. Some anterior axons recross near the AC (arrowheads), whereas others continue contralaterally. Other axons recross in the PC (long arrows). The optic tract is severely defasciculated. (H and I) WT and *ast* optic chiasm. Arrows indicate where axons exit right (red) and left (green) eyes. (I) Axons from both eyes split near the midline (asterisks) into several bundles.

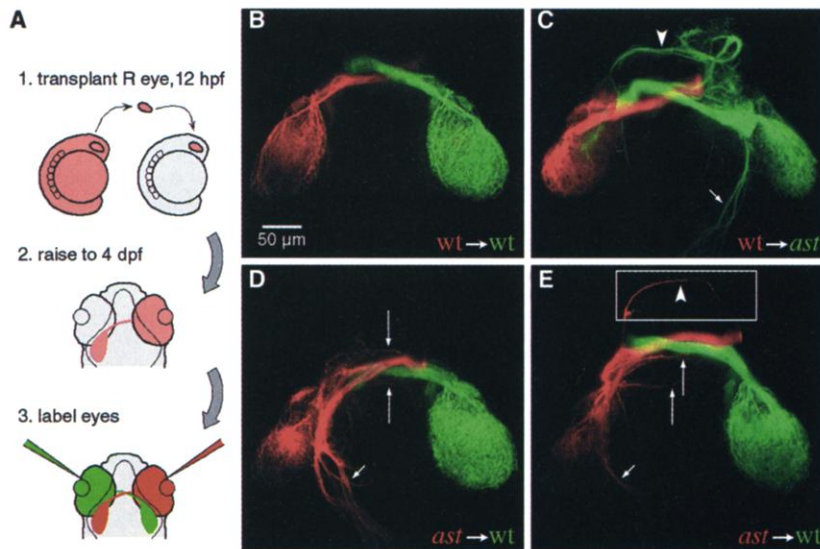


Fig. 2. *ast* is required eye-autonomously. (A) Transplant scheme. (B to E) Retinal projections in chimeric animals; dorsal views. Axons from transplanted eyes are shown in red; axons from host eyes are in green. Boxed inset in (E) is shown at high gain. (B) WT eye in WT host projects normally. (C) WT axons in *ti272z* host project normally despite lack of *ast* function in the brain. *ast* host axons project anteriorly into the diencephalon where they recross the midline (arrowhead), and posteriorly to the VHB (short arrow). (D and E) Two examples of *ti272z* eyes in WT hosts, showing that *ast* axons project aberrantly despite the WT environment. Transplanted *ast* eyes project anteriorly into the diencephalon and across the midline (arrowhead); posteriorly toward the VHB (short arrows); and across the PC (long arrows). WT host axons project normally.

The requirement for *ast* function is highly specific. Overall body shape appears normal, and *ast^{ti272z}* homozygotes are partially adult viable and fertile. The anterior and postoptic commissures form normally (9). Staining *ast^{ti272z}* ($n = 9$) with the zn-5 antibody (10) at 52 hours postfertilization (hpf) showed that *ast* RGC axons oriented locally toward the optic disc and left the eye in a single bundle as in WT (10).

To determine whether *ast* function is required in the eye or in the brain, we used eye transplantation (10) to create chimeric animals with an *ast* mutant eye in an otherwise WT embryo, or vice versa. Eye primordia were transplanted at 12 hpf, immediately after optic vesicle formation and well before retinal axon outgrowth. Both host and transplanted eyes were labeled (Fig. 2A) at 4 dpf, when the retinotectal projection is mature. In controls ($n = 10$), WT eyes in WT hosts showed strong projections to contralateral tectum (10/10 transplants) (Fig. 2B). Occasionally there was a weak projection to ipsilateral tectum (4/10), presumably representing axons that encountered surgically disturbed tissue and were diverted upon exiting the eye. Controls did not show anterior or VHB projections (0/10). WT eyes transplanted into *ast^{ti272z}* homozygotes showed strong contralateral projections (6/6), and no anterior or VHB projections (0/6), despite the mutant environment through which their axons grew (Fig. 2C). In contrast *ast^{ti272z}* eyes transplanted into WT hosts showed a clear *ast* phenotype (Fig. 2, D and E), projecting anteriorly to forebrain (4/8), posteriorly to VHB (8/8), or across the PC (5/8). Thus, *ast* function is required in the eye, most likely in RGC axons.

The *ast* phenotype exhibits similarities to loss-of-function mutations in *Caenorhabditis elegans sax-3* and its *Drosophila* homolog *roundabout (robo)*. *sax-3* mutants show abnormal axon crossing of the ventral nerve cord, abnormal guidance to the ventral nerve cord, anterior and posterior projection defects, and fasciculation defects (12, 13). In *robo* mutants, axons inappropriately cross and recross the CNS midline (14). *sax-3* and *robo* are members of the evolutionarily conserved family of Robo-like receptors with five immunoglobulin (Ig) domains, three fibronectin type III (FNIII) repeats, a single transmembrane domain, and four conserved cytoplasmic motifs. Given the similarity in phenotypes and our eye transplantation results, we examined whether *ast* is a zebrafish *robo*. Our group has cloned three zebrafish *robo* homologs (15), of which one, *robo2* (an ortholog of mammalian *robo2*), is expressed at the appropriate time in RGCs and was therefore a likely candidate for *ast*.

To determine whether the *ast* phenotype could be caused by mutations in *robo2*, we

REPORTS

placed both on the zebrafish genetic map (10, 16, 17). *ast^{ti272z}* mapped to linkage group (LG) 15 between simple sequence repeats (SSRs) z13822 (0.3 cM) and z26441 (0.1 cM) on one side and z7381 (3.8 cM) on the other (Fig. 3A). *robo2* mapped to LG15 on the radiation hybrid (RH) map, 6 cR₃₀₀₀ (centi-Ray 3000) from z13822 (Fig. 3A). The 0.3-cM distance of *ast^{ti272z}* to z13822 corresponds to ~222 kb and the 6 cR₃₀₀₀ distance of *robo2* to z13822 corresponds to ~366 kb [1 cM = ~740 kb (16); 1 cR₃₀₀₀ = ~61 kb (17)]. This linkage supported the possibility that *ast* is *robo2*.

To further examine whether *ast* is *robo2*, we sequenced the *robo2* coding sequence from a strong allele, *ast^{ti272z}*, and a weak allele, *ast^{te284}*, seeking mutations that could account for the *ast* phenotype. Because the

mutations were induced by ethylnitrosourea (18), we expected to find point mutations in the affected gene. Although *robo2* mRNA was detectable at 5 dpf by in situ hybridization, we were unable to produce *robo2* cDNA from phenotypically identified 5-dpf mutants after fixation, embedding, and dye injection. Therefore, we identified homozygous mutant embryos at 36 hpf by genotyping with the closely linked SSR marker z13822. To identify the mutation in *ast^{ti272z}*, we sequenced the *robo2* coding region in two presumed homozygous mutant embryos and one presumed homozygous WT embryo from a *ti272z/+* × *ti272z/+* incross (10). Comparison of *robo2* cDNA sequences revealed four differences between the *ast^{ti272z}* embryos and their WT sibling that cause predicted amino acid changes and were therefore candidates to be the *ast^{ti272z}* mutation.

To distinguish between an induced mutation and naturally occurring polymorphisms, we sequenced the regions of the four candidate changes in genomic DNA from the mutagenized founder fish that gave rise to the *ast^{ti272z}* allele (10). Only one candidate differed between the founder and *ast^{ti272z}*, an A1903T transversion, which is a nonsense mutation changing Arg⁶³⁵ to Stop before the second FNIII repeat (Fig. 3B). The other three candidates were identical between the founder and *ast^{ti272z}* and are therefore naturally occurring polymorphisms between the strains used to generate the *ast^{ti272z/+}* parents. An identical analysis for *ast^{te284}* revealed a G2645A transition, a missense mutation changing Gly⁸⁸² to Asp in the transmembrane domain (Fig. 3B). Three other candidate changes found in the *te284/+* ×

te284/+ incross were identified as naturally occurring polymorphisms. The mutations 1903T and 2645A were only found in *ast^{ti272z}* and *ast^{te284}*, respectively, and in no other clone, and were the only sites where the sequence differed between these two alleles. Taken together, these data show that the *ast* phenotype is caused by mutations in zebrafish *robo2*. The *ast^{ti272z}* allele encodes a truncated Robo2 protein, which could potentially be secreted but cannot function as a receptor, whereas *ast^{te284}* changes an uncharged Gly to a charged Asp in the transmembrane domain.

In situ hybridization for *robo2* with embryos from an *ast^{ti272z}* heterozygous incross revealed a slightly reduced RNA level in 8 of 37 embryos (21.6%) at 36 hpf. Genotyping these embryos with z26441 revealed that those with reduced RNA level were *ast/ast* whereas the rest were *ast/+* ($n = 19$; 51.4%) or *+/+* ($n = 10$; 27.0%). This is consistent with reports that a premature stop codon can cause nonsense-mediated RNA decay (19). No difference in RNA level was detected between 36 hpf embryos of an *ast^{te284}* heterozygous incross.

The *te378* and *tl231* alleles were originally assigned to the same gene as *te284* and *ti272z* (8) by virtue of their similar phenotype and noncomplementation. To rule out the possibility of intergenic noncomplementation, we tested for linkage to *robo2* and found 0 recombinations out of 86 meioses between *ast^{te378}* and z26441, and 0 recombinations between *ast^{tl231}* and z13822 (10). Therefore, we conclude that they are indeed mutant alleles of *robo2*.

To determine when *robo2* could act to

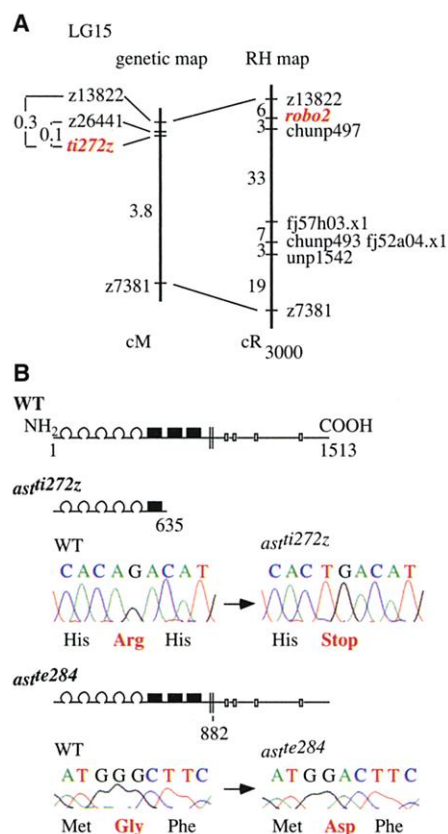


Fig. 3. Cloning of *ast*. (A) *ast^{ti272z}* is tightly linked to *robo2*. *ast^{ti272z}* maps 0.3 cM from z13822 (2 recombinations in 596 meioses), 0.1 cM from z26441 (1 recombination in 762 meioses), and 3.8 cM from z7381 (28 recombinations in 762 meioses). *robo2* maps 6 cR₃₀₀₀ from z13822 on the same side as *ast^{ti272z}*. (B) Identification of mutations in *ast^{ti272z}* and *ast^{te284}*. Schematic representation of zebrafish Robo2: semicircles, Ig domains; filled rectangles, FNIII domains; open rectangles, cytoplasmic motifs. *ast^{ti272z}* encodes an Arg⁶³⁵ to Stop mutation before the second FNIII domain. *ast^{te284}* changes Gly⁸⁸² to Asp in the transmembrane domain. Chromatograms show WT (left) and mutant (right) sequences. Numbers indicate amino acid positions.

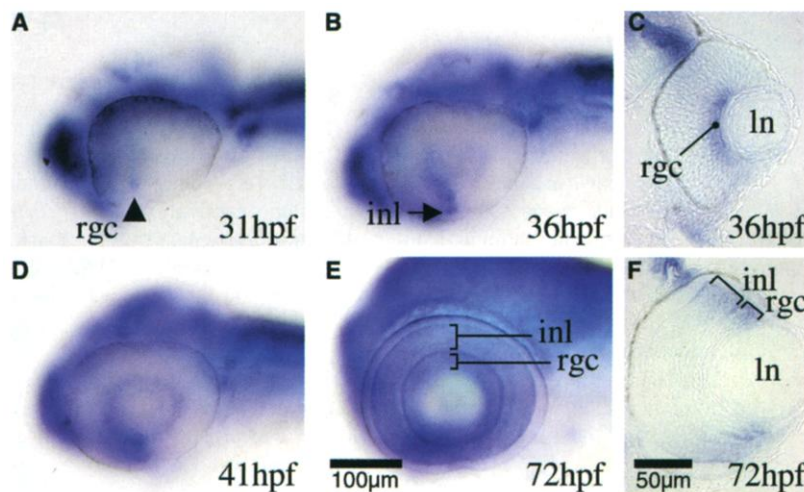


Fig. 4. Spatiotemporal expression of *robo2* mRNA in the eye. (A, B, D, and E) Lateral views between 31 and 72 hpf. (C and F) Transverse sections through the retina at 36 and 72 hpf. (A) A ventronasal patch of RGCs are the first to express *robo2* mRNA at 31 hpf. (B and C) At 36 hpf, expression in the RGC layer has spread dorsally and temporally. RGCs expressing *robo2* are in the central retina (C). A ventronasal patch of cells are the first to express *robo2* in the INL. (D) At 41 hpf, RGC expression has completed a full circle and INL expression has spread nasodorsally. (E and F) At 72 hpf, expression of *robo2* in the RGC layer and INL is detectable in all four retinal quadrants but not in the central retina (F). In, lens.

guide RGC axons, we conducted a detailed spatiotemporal expression analysis using whole-mount in situ hybridization (10). We were unable to detect *robo2* mRNA in the retina at 28 hpf. At 31 hpf, weak expression was detectable in a ventronasal patch of cells adjacent to the ventral fissure (Fig. 4A). These are presumably the first-born RGCs, which appear in this location between 27 and 28 hpf (20) and project axons across the midline at 33 to 35 hpf (21). At 36 hpf (Fig. 4B), the expression had spread dorsally and temporally, reflecting the pattern of early RGC differentiation (20, 21). By 41 hpf, *robo2* was expressed in all quadrants of the RGC layer (Fig. 4, D and E). Although the RGCs expressing *robo2* were initially located centrally (Fig. 4C), expression later became peripherally restricted, and we were unable to detect expression in the older central RGCs at 72 hpf (Fig. 4F). Thus, *robo2* is first expressed in RGCs shortly after their differentiation and turns off later, consistent with what might be expected for an axon guidance receptor. We have not yet successfully generated antibodies to study Robo2 protein regulation. Intriguingly, *robo2* was also expressed at certain points adjacent to the retinotectal projection (10) and in the inner nuclear layer (INL) (Fig. 4, B, E, and F).

Our genetic mapping and allele sequencing data show that the *ast* phenotype is caused by mutations in zebrafish *robo2*. Together with the phenotypic analysis, this shows that *ast/robo2* is essential for establishing the retinotectal projection. Because transplanted *ast^{ti272z}* RGC axons navigate incorrectly in a WT environment, and from its structural similarity to *Drosophila* Robo, we conclude that Ast/Robo2 acts as a guidance receptor in RGC axons. Conversely, because WT axons project normally in an *ast^{ti272z}* host, it is likely that *ast/robo2* function is not required in the environment. The only caveat is that *ast^{ti272z}* homozygotes still express some *robo2* mRNA, and thus could produce a secreted Robo2 fragment encoded by *ast^{ti272z}*. We cannot exclude the possibility that this truncated protein could mimic a normal non-cell autonomous function of Ast/Robo2 and thus guide the transplanted WT axons.

In *Drosophila*, Robo acts as a guidance receptor that recognizes the repulsive signal Slit, produced by midline glia, and prevents inappropriate crossing of the midline (14, 22), whereas the combination of different Robos determines the medial-lateral position of the longitudinal fascicles (23, 24). In zebrafish RGC axon guidance, *ast/robo2* functions not only to prevent inappropriate midline recrossing, but also to form the optic chiasm and prevent abnormal anterior and posterior projections and optic tract defasciculation. The *ast* phenotype is thus more

reminiscent of the *C. elegans sax-3* axon guidance phenotype (12, 13).

Coculture experiments have shown that mammalian Slit2 can repel RGC axons (25), inhibit RGC axon outgrowth (26, 27), and cause tighter fasciculation of retinal axons (27). The complex pattern of *slit1*, *slit2*, and *slit3* expression along the optic pathway suggested that mammalian Slits might guide retinal axons at positions other than the midline (25–27). From its expression in RGCs, mammalian Robo2 is likely to be the receptor that mediates their response to Slits (26, 27). Together with preliminary observations that two zebrafish Slits are expressed along the optic pathway (28), our Astray/Robo2 functional data suggest a conserved role for this ligand-receptor system in the vertebrate visual system.

References and Notes

1. D. D. O'Leary, D. G. Wilkinson, *Curr. Opin. Neurobiol.* **9**, 65 (1999).
2. U. Drescher, F. Bonhoeffer, B. K. Müller, *Curr. Opin. Neurobiol.* **7**, 75 (1997).
3. A. Brown *et al.*, *Cell* **102**, 77 (2000).
4. M. S. Deiner *et al.*, *Neuron* **19**, 575 (1997).
5. E. Birgbauer, C. A. Cowan, D. W. Sretavan, M. Henkemeyer, *Development* **127**, 1231 (2000).
6. K. Kruger, A. S. Tam, C. Lu, D. W. Sretavan, *J. Neurosci.* **18**, 5692 (1998).
7. S. Nakagawa *et al.*, *Neuron* **25**, 599 (2000).
8. H. Baier *et al.*, *Development* **123**, 415 (1996).
9. R. O. Karlstrom *et al.*, *Development* **123**, 427 (1996).

10. Supplementary data are available on Science Online at www.sciencemag.org/cgi/content/full/292/5516/507/DC1.
11. C.-B. Chien, unpublished data.
12. J. A. Zallen, B. A. Yi, C. I. Bargmann, *Cell* **92**, 217 (1998).
13. J. A. Zallen, S. A. Kirch, C. I. Bargmann, *Development* **126**, 3679 (1999).
14. T. Kidd *et al.*, *Cell* **92**, 205 (1998).
15. J.-S. Lee, R. Ray, C.-B. Chien, *Dev. Dyn.*, in press.
16. N. Shimoda *et al.*, *Genomics* **58**, 219 (1999).
17. R. Geisler *et al.*, *Nature Genet.* **23**, 86 (1999).
18. P. Haffter *et al.*, *Development* **123**, 1 (1996).
19. M. W. Hentze, A. E. Kulozik, *Cell* **96**, 307 (1999).
20. M. Hu, S. S. Easter Jr., *Dev. Biol.* **207**, 309 (1999).
21. J. D. Burrill, S. S. Easter Jr., *J. Neurosci.* **15**, 2935 (1995).
22. T. Kidd, K. S. Bland, C. S. Goodman, *Cell* **96**, 785 (1999).
23. J. H. Simpson, K. S. Bland, R. D. Fetter, C. S. Goodman, *Cell* **103**, 1019 (2000).
24. S. Rajagopalan, V. Vivancos, E. Nicolas, B. J. Dickson, *Cell* **103**, 1033 (2000).
25. S. P. Niclou, L. Jia, J. A. Raper, *J. Neurosci.* **20**, 4962 (2000).
26. L. Erskine *et al.*, *J. Neurosci.* **20**, 4975 (2000).
27. T. Ringstedt *et al.*, *J. Neurosci.* **20**, 4983 (2000).
28. L. Hutson, M. Juryneć, C.-B. Chien, unpublished data.
29. We dedicate this work to P. Haffter, mentor and friend. We thank M. Condic, D. Grunwald, L. Hutson, and A. Pittman for helpful comments on the manuscript; B. Grunewald, A. Kugath, and B. Wooldridge for technical assistance; and N. Marsh-Armstrong for advice on eye transplants. C.F. thanks T. Roeser for support. Supported by Deutscher Akademischer Austauschdienst fellowship #D/99/14906 (C.F.), European Molecular Biology Organization fellowship ALTF 350-1995 (C.-B.C.), a University of Utah seed grant (C.-B.C.), and NIH grant R01-EY12873 (C.-B.C.).

1 February 2001; accepted 19 March 2001

Fast Backprojections from the Motion to the Primary Visual Area Necessary for Visual Awareness

Alvaro Pascual-Leone^{1*} and Vincent Walsh²

Much is known about the pathways from photoreceptors to higher visual areas in the brain. However, how we become aware of what we see or of having seen at all is a problem that has eluded neuroscience. Recordings from macaque V1 during deactivation of MT+/V5 and psychophysical studies of perceptual integration suggest that feedback from secondary visual areas to V1 is necessary for visual awareness. We used transcranial magnetic stimulation to probe the timing and function of feedback from human area MT+/V5 to V1 and found its action to be early and critical for awareness of visual motion.

Two hypotheses that were postulated about how brain activity mediates awareness have particular relevance to neurophysiology (1–4). There might be a class of neurons or

neural pathways whose activity mediates awareness. Alternatively, awareness might be the result of specific forms of neuronal activity such as synchronous discharges or spike rate modulations. These hypotheses are not mutually exclusive, and a combination of both might be proposed (4). The role of striate cortex (V1) in visual awareness (4–8) is controversial; it may not have specialized “awareness-dedicated” neurons, but the spiking rate of V1 neurons appears to be modulated by perceptual context, correlated with

¹Laboratory for Magnetic Brain Stimulation, Beth Israel Deaconess Medical Center, Harvard Medical School, 330 Brookline Avenue, Kirsstein Hall K5454, Boston MA 02115, USA. ²Experimental Psychology, University of Oxford, South Parks Road, Oxford OX1 3UD, UK.

*To whom correspondence should be addressed. E-mail: apleone@caregroup.harvard.edu